

Transient Absorption Spectroscopy and Imaging of Individual Chirality-Assigned Single-Walled Carbon Nanotubes

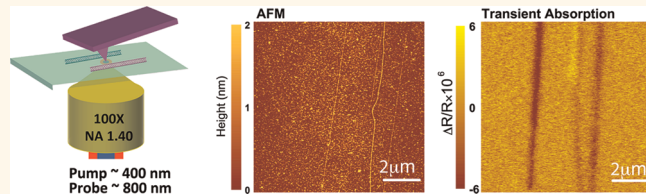
Bo Gao,[†] Gregory V. Hartland,[‡] and Libai Huang^{†,*}

[†]Radiation Laboratory, University of Notre Dame, Notre Dame, Indiana 46556, United States and [‡]Department of Chemistry and Biochemistry, University of Notre Dame, Notre Dame, Indiana 46556, United States

Single-walled carbon nanotubes (SWNTs) are novel one-dimensional (1D) nano-materials that can be considered as graphene layers rolled up to form cylinders.¹ A SWNT can be either semiconducting or metallic depending on its diameter and rolling angle.^{2,3} Extensive research efforts have been made to measure and model their physical properties and to develop their unique traits for applications.^{4–5} However, understanding of the intrinsic optical properties of SWNTs has been hindered by the distribution of semiconducting and metallic tube types in as-synthesized samples. This difficulty can be circumvented to a certain extent by encapsulating individual SWNTs in surfactant micelles⁶ and more recently using size-selective separation techniques to enrich a single chirality.^{7,8} Initial experiments performed with these samples demonstrated near-IR fluorescence originating from semiconducting SWNTs.^{6,9–11} Subsequently, various optical studies such as ultrafast spectroscopy,^{12–18} two-photon photoluminescence,¹⁹ and temperature-dependent fluorescence lifetime spectroscopy^{11,20} have revealed that excitons rather than free electrons and holes correctly account for the excited states of SWNTs. These studies show that the excitonic structure of SWNTs is complex: there are four singlet excitons ($e-h$ pair excitations) for each matching pair of van Hove singularities (E_{ii}), but only one is optically bright.^{21–25}

Time-resolved studies of purified SWNT samples have significantly improved our understanding of exciton structure and dynamics.^{12–18} However, questions remain about the intrinsic optical properties of SWNTs. One outstanding question is the origin of the excited-state absorption of SWNTs. Photoinduced absorption bands have been observed in SWNT suspensions,^{26–29} films,¹² and composites.^{30,31} A variety of

ABSTRACT



Femtosecond transient absorption microscopy was employed to study the excited-state dynamics of *individual* semiconducting single-walled carbon nanotubes (SWNTs) with simultaneously high spatial (~ 200 nm) and temporal (~ 300 fs) resolution. Isolated SWNTs were located using atomic force microscopy, and Raman spectroscopy was employed to determine the chiral index of select nanotubes. This unique experimental approach removes sample heterogeneity in ultrafast measurements of these complex materials. Transient absorption spectra of the individual SWNTs were obtained by recording transient absorption images at different probe wavelengths. These measurements provide new information about the origin of the photoinduced absorption features of SWNTs. Transient absorption traces were also collected for individual SWNTs. The dynamics show a fast, ~ 1 ps, decay for all the semiconducting nanotubes studied, which is significantly faster than the previously reported decay times for SWNT suspensions. We attributed this fast relaxation to coupling between the excitons created by the pump laser pulse and the substrate.

KEYWORDS: ultrafast pump–probe spectroscopy · transient absorption microscopy · single-walled carbon nanotubes · excited-state dynamics · excited-state absorption

mechanisms have been invoked to explain the spectra, such as intersubband exciton transitions,¹² carrier-induced absorption broadening,²⁶ and the formation of biexcitons.³¹ However, overlapping contributions from different tube types in addition to the inherently complex exciton structure prevent conclusive assignment of features in the transient absorption spectra of polydispersed SWNT samples. Recently, ultrafast spectroscopy has been performed on enriched (6,5) SWNT suspensions,^{28,29} but even single-chirality samples can contain small bundles and trace amount of other

* Address correspondence to lhuang2@nd.edu.

Received for review February 20, 2012 and accepted May 13, 2012.

Published online May 13, 2012
10.1021/nn300753a

© 2012 American Chemical Society

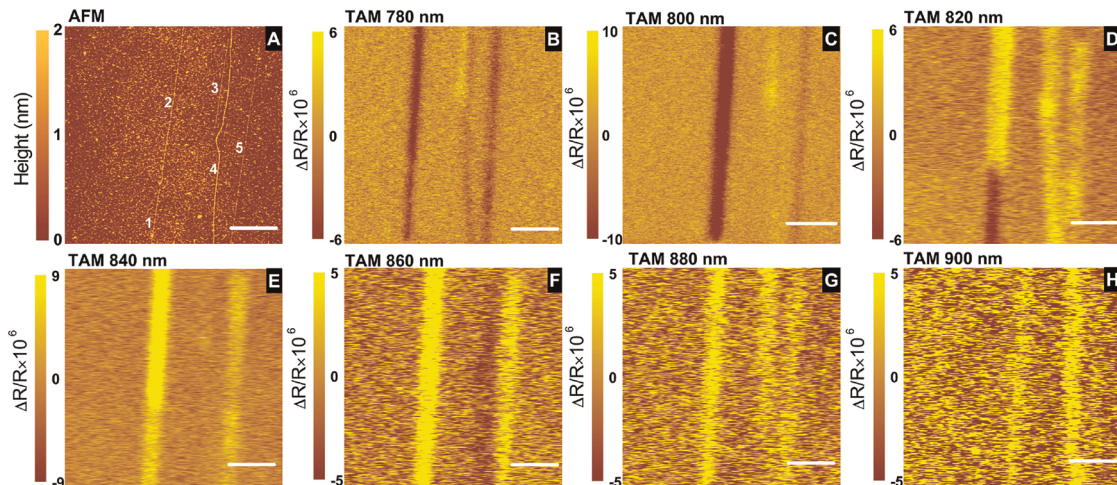


Figure 1. (A) Tapping mode AFM height image of SWNT-1, -2, -3, -4, and -5. (B to H) Transient absorption microscopy (TAM) images with pump/probe wavelengths of 390/780, 400/800, 410/820, 420/840, 430/860, 440/880, and 450/900 nm, respectively. All TAM images were collected at a pump–probe delay of 0 ps. Note that the scale of the reflectivity change is different for each TAM image. Scale bars are 2 μ m in all images.

chiralities.^{7,8} The intrinsic optical properties can also be altered by the extensive sample processing required to purify SWNTs. For instance, the harsh acid treatments and ultrasonic processing that are used in most suspension procedures damage the SWNT sidewalls, shorten the length of the nanotubes, and lead to additional nonradiative pathways.³²

These issues point to the need to perform ultrafast spectroscopy on individual as-grown SWNTs. This can be achieved using transient absorption microscopy, where a high-sensitivity ultrafast laser system is coupled to an optical microscope, allowing measurements with simultaneous high spatial and temporal resolution. This technique has been used to study single metal and semiconductor nanostructures^{33–36} and offers distinct advantages over fluorescence-based methods, where only materials with high emission quantum yields can be studied. Single chemical vapor deposition (CVD)-grown SWNTs and surfactant-encapsulated SWNTs were recently imaged through transient absorption microscopy by Jung *et al.*³⁷ However, the dynamics traces reported in ref 37 were with a time resolution of \sim 5 ps, which is insufficient to resolve the fast relaxation processes that have been observed in solution phase ensemble measurements.^{13–18} Four-wave mixing techniques have also been employed to image individual SWNTs;^{38,39} however, limited dynamics information was obtained from these studies.

In this work, we report transient absorption microscopy experiments on individual semiconducting SWNTs with known chiralities grown by CVD. We construct transient absorption spectra of individual SWNTs by scanning the probe wavelength around the E_{22} exciton resonances, where photoinduced bleach and absorption features relating to the electronic structure of the individual semiconducting SWNTs were observed. A fast, \sim 1 ps relaxation process dominates the transient

absorption decays of the individual nanotubes on glass substrates. By comparing our results to previous studies in SWNT suspensions,^{13,14,16–18} we ascribed this fast relaxation to the coupling of the excited states of the SWNTs to the substrate.

RESULTS AND DISCUSSION

Figure 1A shows the atomic force microscopy (AFM) height image of a $10 \times 10 \mu\text{m}$ region of the sample, where five SWNTs are visible. The SWNTs are labeled as SWNT-1, -2, -3, -4, and -5. Raman measurements show that SWNT-1 and SWNT-2 are two separate tubes: two distinct radial breathing mode (RBM) peaks were clearly resolved; see Figure 2. Two other SWNTs, SWNT-6 and -7, were also investigated, and an AFM image of these nanotubes is shown in the Supporting Information (Figure S1A). Raman spectra (Figure 2 and Figure S2) with 785 nm excitation showed RBM frequencies of 185.0, 181.1, 120.0, and 210.6 cm^{-1} for SWNT-1, -2, -5, and -6, corresponding to diameters of 1.30, 1.34, 2.06, and 1.12 nm, respectively.⁴⁰ No RBMs were observed for SWNT-3, -4, and -7, probably because their RBM frequencies are $<100 \text{ cm}^{-1}$, which is outside our detection window.

Because only SWNTs with electronic resonances near the laser excitation have detectable RBM signals, we used the RBM frequency in combination with the resonance conditions to assign chirality.⁴⁰ For example, SWNT-6 has a RBM frequency of 210.6 cm^{-1} . There are two SWNT chiralities that have RBM frequencies within 1 cm^{-1} (the resolution of our instrument) of 210.6 cm^{-1} . These are a semiconducting SWNT with a chiral index of (13,2) and a metallic SWNT with a chiral index of (11,5). The (13,2) SWNT has an E_{22} resonance at 1.45 eV, which is close to the Raman laser (1.58 eV). In contrast, the closest resonance to the Raman laser for the (11,5) SWNT is the E_{11} resonance at 1.99 eV, which is too far

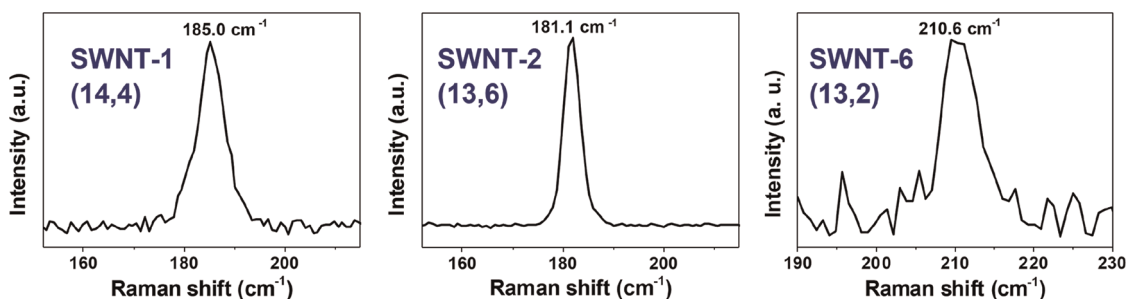


Figure 2. Raman spectra of SWNT-1, -2, and -6 with an excitation wavelength of 785 nm.

TABLE 1. RBM Frequencies, Chiral Index, and the First (E_{11}), Second (E_{22}), Third (E_{33}), and Fourth (E_{44}) Exciton Level Energies for SWNT-1, -2, and -6

SWNT	RBM (cm^{-1})	chiral index ^{41,42}	E_{11} (eV) ^{41,42}	E_{22} (eV/nm) ^{41,42}	E_{33} (eV) ^{43,44}	E_{44} (eV) ^{43,44}
SWNT-1	185.0	(14, 4)	0.764	1.472/842	2.438	3.014
SWNT-2	181.1	(13, 6)	0.760	1.419/874	2.438	2.900
SWNT-6	210.6	(13, 2)	0.949	1.446/857	2.994	2.826

away to generate a strong Raman signal.^{40,41} Therefore, we assign the chirality of SWNT-6 to (13,2). Similarly, SWNT-2 was assigned to (13,6) and SWNT-1 was assigned to (14,4). The chiral index and the energies of the bright excitons associated with the first (E_{11}), second (E_{22}), third (E_{33}), and fourth (E_{44}) subbands are summarized in Table 1 for SWNT-1, -2, and -6. Values of E_{11} and E_{22} were obtained from experimental photoluminescence data reported in refs 41 and 42, while E_{33} and E_{44} values were obtained from calculations presented in refs 43 and 44.

For SWNT-5, a RBM frequency of 120.0 cm^{-1} was observed (Figure S2). A conclusive assignment for SWNT-5 is not possible due to its larger diameter (2.06 nm). However, on the basis of resonance conditions it can be assigned to a semiconducting nanotube. Specifically, for a metallic SWNT with a diameter of $\sim 2.06\text{ nm}$, the E_{11} resonance is at $\sim 1.2\text{ eV}$,⁴⁰ much lower than the laser excitation energy. On the other hand, the E_{33} resonance for semiconducting SWNTs with diameters of 2.06 nm is $\sim 1.5\text{ eV}$,⁴⁰ which is much closer to the Raman laser excitation energy. SWNT-5 could be one of the following five chiralities: (25, 2), (21, 8), (16, 14), (17, 13), or (19, 11).

Figure 1B–H show transient absorption microscopy (TAM) images of the same sample area in Figure 1A at pump/probe wavelengths of 390/780, 400/800, 410/820, 420/840, 430/860, 440/880, and 450/900 nm. The TAM images for SWNT-6 and -7 are shown in the Supporting Information (Figure S1). All TAM images were collected at a pump–probe delay of 0 ps. In these experiments the probe wavelength is close to the E_{22} transition and the pump wavelength is close to the E_{44} transition of SWNT-1, -2, and -6. Wavelength-dependent transient absorption signals are observed from all seven

individual SWNTs investigated. When probing at 780 nm (Figure 1B), SWNT-1, -2, -4, and -5 exhibit negative $\Delta R/R$ signals, meaning less reflection of the probe with the presence of the pump, which corresponds to a photoinduced absorption (PA) signal. In contrast, SWNT-3 shows a positive transient reflectivity ($\Delta R/R$), corresponding to a photoinduced bleach (PB) signal at this wavelength. As the probe wavelength changes, $\Delta R/R$ exhibits changes in both magnitude and sign. For example, $\Delta R/R$ of SWNT-2 is negative (PA) at 800 nm and turns positive (PB) at 820 nm.

The transient absorption spectra for six SWNTs (-1, -2, -4, -5, -6, and -7) at 0 ps delay time are presented in Figure 3, and the spectrum for SWNT-3 is shown in Figure S3. For SWNT-1, PA occurs at wavelengths of 820 nm and shorter with a maximum around 800 nm, while a PB band is observed at longer wavelength with a peak around 860 nm. SWNT-2 exhibits a trend similar to that of SWNT-1, with a blue-shifted PA band relative to the PB band. For SWNT-6 and -7, the PA band is redshifted relative to the PB band, in contrast to that for SWNT-1 and -2. The magnitude of the PA signal at 900 nm for SWNT-6 is significantly larger than the signal at other wavelengths, probably because the pump (450 nm) is resonant with the E_{44} transition for this nanotube. SWNT-5 shows a transient absorption spectrum very similar to those of SWNT-1 and -2, but with smaller amplitude. The transient absorption spectrum of SWNT-4 oscillates between PA and PB. No detectable signal was found for SWNT-3 for wavelengths longer than 820 nm, and a PB band is observed for wavelengths shorter than 820 nm (Figure S3).

The excited-state dynamics of the individual SWNTs were also studied, and transient absorption decay traces from SWNT-2 and SWNT-1 are shown in Figure 4 and Figure S4, respectively. Figure 4A shows the kinetics taken at the maximum of the PB band (840 nm), and Figure 4B shows data collected at the PA band (800 nm). To avoid carbon deposition onto the sample, a pump intensity of $16\mu\text{J}/\text{cm}^{-2}$ (< 1 exciton per 30 nm) or lower was used for collecting kinetics. The decays are extremely fast, with signals fully recovered within a few picoseconds. A single-exponential decay convoluted with a Gaussian response function was employed to fit the traces and gave decay constants of 0.9 ± 0.1 for

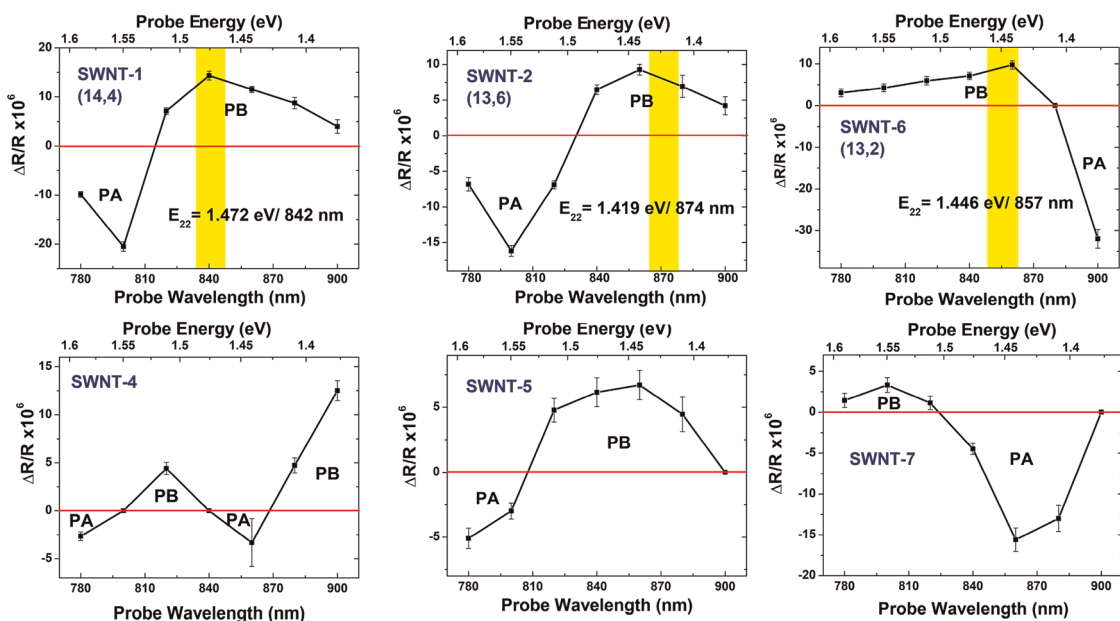


Figure 3. Transient reflectivity changes ($\Delta R/R$) at 0 ps pump–probe delay time *versus* probe wavelength for SWNT-1, -2, and -6 and SWNT-4, -5, and -7. For SWNT-1, -2, and -6, the chirality assignments are indicated. The yellow bars with a width of 25 meV correspond to the position of the E_{22} exciton resonances of SWNT-1, -2, and -6. PA = photoinduced absorption; PB = photoinduced bleach.

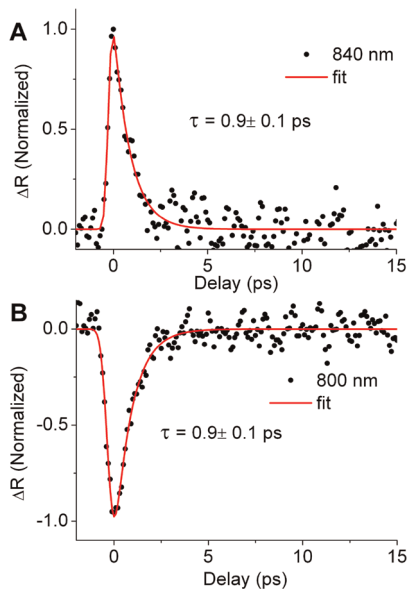


Figure 4. Transient absorption traces for SWNT-2 at pump/probe wavelengths of (A) 420/840 nm and (B) 400/800 nm. A pump intensity of $16 \mu\text{J}/\text{cm}^2$ was employed. The traces were fitted with a single-exponential decay convoluted with a Gaussian response function (350 fs fwhm). Experimental data are black circles, and fits are red solid lines.

both the PB and PA bands. Similar decay constants were found for SWNT-1 and -6.

In the following, we discuss the origins of the SWNT structure-specific PA and PB features and the fast dynamics observed for both features. In our experiments, the pump laser creates E_{44} excitons that rapidly relax to the E_{11} level within 100 fs (shorter than the pulse width of the experiments).³⁰ This process reduces

the population of the ground state and increases the population of the low-lying levels in the E_{11} manifold of states. This causes a PB signal for probe transitions that originate from the ground state. For SWNT-1, -2, and -6 the PB bands observed near 850 nm can be attributed to the bleach of the E_{22} exciton resonances. As shown in Figure 3, the positions of the PB bands in these SWNTs agree reasonably well with the E_{22} frequencies measured by photoluminescence.^{41,42} For the larger diameter SWNT-5, the PB band at 850 nm most likely corresponds to the E_{33} resonance.

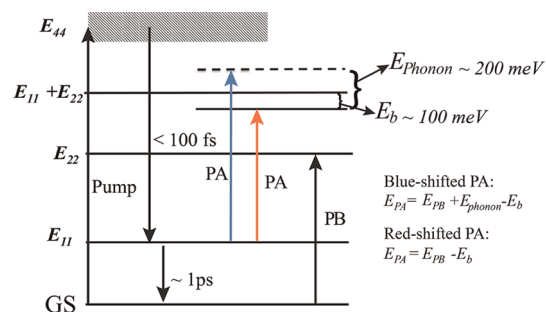
The rapid relaxation to the E_{11} manifold means that the dynamics probed at the PB band should reflect ground-state recovery from the E_{11} level. For semiconducting SWNTs suspended in solution, an initial subpicosecond decay followed by slower decays on the order of tens of picoseconds were observed when probing at the E_{11} and E_{22} resonances.^{13,14} The slow decays were ascribed to recombination of E_{11} excitons, while the origin of the initial fast decay is still under debate.^{13,14,18} For all the individual SWNTs interrogated here, we observe only a fast, ~ 1 ps decay even when probing resonantly at the PB band. We attribute this decay to an additional relaxation pathway introduced by the substrate. Fast energy transfer to the substrate is consistent with the observation of fluorescence quenching for substrate-supported SWNTs.⁴⁵ In principle, exciton–exciton annihilation can also contribute to the fast (~ 1 ps) dynamics in our experiments, especially given that multiexciton generation has been observed with photoexcitation near E_{44} .⁴⁶ However, exciton–exciton annihilation will leave the system in the E_{11} state, and the data in Figure 4 show that the

relaxation of this state is much faster than that observed in solution (~ 10 ps).^{13,14} The intensity dependence of the decay dynamics was also explored. Traces for SWNT-1 at two different pump intensities (8 and $16 \mu\text{J}/\text{cm}^{-2}$) are given in Figure S4. No significant pump intensity dependence was observed, implying that exciton–exciton annihilation is negligible at the pump intensities employed in these measurements.

The origin of the PA features is more complex. Typically PA bands result when the probe is resonant to transitions that originate from an excited state. Korovyanko *et al.* ascribed PA bands in SWNTs films to intersubband excitonic transitions,¹² while Ostojic *et al.* attributed PA bands in micelle-encapsulated SWNT suspensions to carrier-induced absorption broadenings.²⁶ Styers-Barnett *et al.* performed experiments with SWNT mixtures embedded in polymer matrices and argued that red-shifted PA bands resulted from the formation of biexcitons.³¹ Ambiguity exists in assigning PA features in these polydispersed samples, because the bands of one tube type can overlap with bands of another tube type. Recently, transient absorption spectra of enriched (6,5) SWNT suspensions showed only blue-shifted PA bands near both the E_{11} and E_{22} transitions.^{28,29} The blue-shifted PA band near the E_{11} resonance was attributed to transitions from the dark singlet exciton in the E_{11} manifold to a state in the $E_{11} + E_{11}$ biexciton manifold.^{28,29}

Our measurements unambiguously demonstrate that the position of the PA bands is chirality dependent and can be either blue- or red-shifted relative to the E_{22} exciton resonance. Specifically, the PA feature is blue-shifted for SWNT-1, -2, and -5 and red-shifted for SWNT-6 and -7. This rules out the carrier-induced peak-broadening mechanism, because peak broadenings result in symmetrical PA bands on either side of the PB band. Because population in the higher excitonic levels relaxes to the E_{11} subband within the laser pulse, only transitions originating from the E_{11} exciton manifold can contribute to the observed PA signal. For SWNT-1, transitions from E_{11} to E_{22} , E_{33} , and E_{44} have energies of ~ 0.7 , ~ 1.7 , and 2.3 eV, respectively, while the PA band centers at ~ 1.55 eV. For SWNT-2, the PA position and the interband transition energies are similar to those of SWNT-1 (Table 1). For SWNT-6, the PA band occurs at ~ 1.38 eV, while transition energies from E_{11} to E_{22} , E_{33} , and E_{44} are ~ 0.5 , 2.0 , and 1.9 eV, respectively. Thus, interband transitions originating from E_{11} do not have the correct energies to explain the observed PA band positions, which rules out intersubband transitions as a possible mechanism for the PA signal.

On the basis of these considerations, we assign the PA features to transitions from the lowest level in the E_{11} exciton manifold to levels in the $E_{11} + E_{22}$ biexciton manifold. Theoretical calculations predicted biexciton binding energy (E_b) in semiconducting SWNTs to be



Scheme 1. Summary of the relaxation processes involved in transient absorption measurements on SWNTs. After excitation by the pump pulse the system rapidly relaxes (< 100 fs) to the lowest energy level of the E_{11} manifold. PB features result from the pump-induced bleach of the E_{22} transition. PA bands arise from transitions from the E_{11} manifold to the $E_{11} + E_{22}$ manifold. E_b represents the biexciton binding energy. The energy level diagram illustrates the blue-shifted and red-shifted PA signals. The red-shifted PA feature is due to the finite binding energy of the biexciton state. The blue-shifted PA bands correspond to phonon-assisted transitions, where E_{phonon} is the phonon energy

substantial, ranging from 50 to 200 meV depending on the SWNT size and the dielectric environment.^{47,48} Thus, transition to the lowest level (s state) of the $E_{11} + E_{22}$ biexciton should produce red-shifted PA bands (Scheme 1), which is observed for SWNT-6 and -7. Within this scheme, the energy of the red-shifted PA feature is given by $E_{\text{PA}} = E_{\text{PB}} - E_b$. The data in Figure 3 give an E_b value of ~ 100 meV for SWNT-7 and $E_b > 80$ meV for SWNT-6 (the limited spectral window of the experiment prevents a more accurate value from being determined for SWNT-6). These E_b values agree well with previous theoretical predictions.^{47,48}

The blue-shifted PA features observed for SWNT-1 and -2 should correspond to transitions to higher levels in the $E_{11} + E_{22}$ manifold; these could be either phonon-assisted transitions^{49,50} or higher exciton levels (p states). The energy splitting between s and p states is on the order of 300 meV for SWNTs with a diameter of ~ 1 nm,¹⁹ which is too large to account for the energy difference between the blue-shifted PA and the PB bands. To account for the ~ 100 meV energy difference between the blue-shifted PA and the PB bands, we consider phonon-assisted formation of biexcitons. From Scheme 1, the energy of the phonon responsible for the blue-shifted PA transition is $E_{\text{phonon}} = E_{\text{PA}} - E_{\text{PB}} + E_b$. This gives a value of $E_{\text{phonon}} \approx 200$ meV, which agrees well with the energy of the G mode optical phonons in SWNTs. The G mode optical phonons are known to couple strongly to electrons and are responsible for absorption side bands observed in previous photoluminescence excitation studies.^{20,49} Therefore, we attribute the blue-shifted PA features to formation of a biexciton assisted by the G mode optical phonons. Relaxation from the higher excited states created by the pump pulse to the E_{11} manifold creates a large population of optical

phonons, which increases the probability of phonon-assisted transitions leading to the blue-shifted PA features.

In principle, every SWNT should show a red-shifted PA feature corresponding to a transition to the $E_{11} + E_{22}$ exciton because of the finite biexciton binding energy. The fact that red-shifted PA features are not observed in all cases is probably due to the limited tuning range of the laser used for these experiments (~ 120 nm). Our results are consistent with the complex excited-state absorption spectra reported for (6,5) enriched samples, where multiple red-shifted and blue-shifted PA bands were observed near the E_{22}^S resonance.⁵⁰ In the experiments presented in ref 50 the position of the PA bands was found to coincide with the phonon side bands observed in photoluminescence excitation measurements.⁵⁰

Our observation of probe wavelength dependent transient absorption signals is in contrast to what have been reported in refs 37 and 51. In these experiments the sign of the transient absorption signals did not change with wavelength, for both metallic and semiconducting surfactant-encapsulated SWNTs.^{37,51} Changes in the sign of the signal are expected when scanning across an electronic resonance, because the PB and PA features in general occur at different wavelengths. However, inhomogeneous broadening can occur in SWNT bundles, washing out resonances of individual

nanotubes and resulting in broad spectral features. Thus, a possible reason for the difference between the results reported here and those in refs 37 and 51 is that Tong *et al.* were interrogating bundles rather than individual SWNTs.

CONCLUSION

In conclusion, we have performed transient absorption microscopy studies on CVD-grown individual SWNTs with known chiralities. By combining diffraction-limited spatial resolution and subpicosecond time resolution, our experiments provided the first measurement of femtosecond excited-state dynamics and transient absorption spectra of individual SWNTs. The transient absorption spectra can be understood as arising from a PB feature due to the ground state to E_{22} transition, and a PA feature to transition from the lowest level in the E_{11} exciton manifold to in the $E_{11} + E_{22}$ biexciton manifold. The PA and PB signals decay on a subpicosecond time scale, due to fast energy transfer from the nanotubes to the substrate. Our unique experimental approach provides a means to remove inhomogeneity and unravel environmental effects in excited-state dynamics of SWNTs. In order to interrogate the intrinsic nonradiative pathways, and to explore differences between different excited states, experiments on suspended individual SWNTs are currently being performed.

EXPERIMENTAL DETAILS

Growth of Individual Carbon Nanotubes. Highly oriented SWNTs with lengths from tens to hundreds of micrometers were grown on single-crystal ST-cut quartz (Hoffman Materials Inc.) with CoCl_2 as the catalyst. The growth was performed in a tube furnace at 870 °C with a flow of methane (1000 sccm) and hydrogen (140 sccm) for 30 min.⁵² SWNTs were subsequently transferred onto a patterned glass coverslip⁵³ in order to correlate Raman spectra and AFM measurements to the transient absorption experiments. Raman spectra of individual SWNTs were collected by a Renishaw Raman microscope (RM1000) with a 785 nm laser as the excitation source.

Transient Absorption Microscopy. Correlated transient absorption microscopy and atomic force microscopy measurements were performed by coupling a Ti:Sapphire oscillator (76 MHz repetition rate, Coherent Mira 900) with a Veeco Bioscope II AFM (operated in tapping mode for height imaging) mounted on an inverted microscope (Nikon Ti-U).³⁶ The tunable output (700–1000 nm) from the Ti:Sapphire oscillator was split into two beams, one of which was employed as the probe and the other was doubled by a β -barium borate crystal to serve as the pump. The polarizations of the pump and probe beams were made parallel to the long axis of the SWNTs. The collinear pump and probe beams were focused at the sample with a 100 \times , 1.40 numerical aperture oil-immersion objective (Nikon Apo). The reflected beams were collected by the same objective, and the probe was detected with an Avalanche photodiode (Hamamatsu C5331-04).

Pump-induced changes in the probe reflectance (ΔR) were measured by modulating the pump beam at 500 kHz with an acousto-optic modulator (IntraAction Corp., AOM-40AF Series) and monitoring the output of the APD with a lock-in amplifier (Zurich Instruments). TAM images were constructed by raster

scanning the sample with a piezo stage (Veeco Bioscope II) and recording the relative change in reflection ($\Delta R/R$) at fixed delay times. The spot size of the pump at the sample was ~ 200 nm, and the spot size of the probe was ~ 400 nm, giving an overall spatial resolution of ~ 200 nm in these images. All TAM images were acquired at a pump–probe delay of 0 ps and with a pump intensity of 0.1 mJ/cm² at the sample. For a pump wavelength at 420 nm, this pump intensity corresponds to a fluence of 2.2×10^{14} photons/cm². Using a resonant absorption cross-section of 90 nm² per μm for 1 nm diameter SWNTs,⁵⁴ we calculate an upper limit for the exciton density of ~ 1 exciton per 5 nm of tube length. Transient absorption traces were obtained by delaying the probe with respect to the pump with a mechanical translation stage (Newport Corp) and recording signals from fixed positions. A lower pump fluence of 16 $\mu\text{J}/\text{cm}^2$ (<1 exciton per 30 nm tube length) or lower was used for the dynamics measurements. For all measurements, the samples were placed under a continuous flow of argon gas to prevent damage. The time resolution at the sample was ~ 350 fs for these experiments. In principle, pump–probe microscopy experiments can be complicated by the thermal lensing effect; however, this is not a problem for resonant signals in nanostructures. In addition, thermal lensing is typically a long time signal, which does not appear in our data.

Conflict of Interest: The authors declare no competing financial interest.

Acknowledgment. B.G. and L.H. acknowledge support from the Office of Basic Energy Science of the U.S. Department of the Energy (DE-FC02-04ER15533). G.V.H. acknowledges the support from the National Science Foundation through award CHE-1110560. This publication is contribution no. NDRL 4903 from the Notre Dame Radiation Laboratory.

Supporting Information Available: Raman spectra of the SWNT-5 as well as AFM and transient absorption microscopy images of the SWNT-6 and -7; transient absorption spectrum of SWNT-3; and pump intensity dependence of transient absorption dynamics of SWNT-1. This material is available free of charge via the Internet at <http://pubs.acs.org>.

REFERENCES AND NOTES

1. Iijima, S.; Ichihashi, T. Single-Shell Carbon Nanotubes of 1-nm Diameter. *Nature* **1993**, *363*, 603–605.
2. Saito, R.; Dresselhaus, G.; Dresselhaus, M. *Physical Properties of Carbon Nanotubes*; Imperial College Press: London, 1998.
3. Ouyang, M.; Huang, J. L.; Lieber, C. M. Fundamental Electronic Properties and Applications of Single-Walled Carbon Nanotubes. *Acc. Chem. Res.* **2002**, *35*, 1018–1025.
4. Baughman, R. H.; Zakhidov, A. A.; de Heer, W. A. Carbon Nanotubes—the Route toward Applications. *Science* **2002**, *297*, 787–92.
5. Avouris, P.; Freitag, M.; Perebeinos, V. Carbon-Nanotube Photonics and Optoelectronics. *Nat. Photon* **2008**, *2*, 341–350.
6. O'Connell, M.; Bachilo, S.; Huffman, C.; Moore, V.; Strano, M.; Haroz, E.; Rialon, K.; Boul, P.; Noon, W.; Kittrell, C.; et al. Band Gap Fluorescence from Individual Single-Walled Carbon Nanotubes. *Science* **2002**, *297*, 593–596.
7. Zheng, M.; Jagota, A.; Strano, M. S.; Santos, A. P.; Barone, P.; Chou, S. G.; Diner, B. A.; Dresselhaus, M. S.; McLean, R. S.; Onoa, G. B.; et al. Structure-Based Carbon Nanotube Sorting by Sequence-Dependent DNA Assembly. *Science* **2003**, *302*, 1545–1548.
8. Arnold, M. S.; Green, A. A.; Hulvat, J. F.; Stupp, S. I.; Hersam, M. C. Sorting Carbon Nanotubes by Electronic Structure Using Density Differentiation. *Nat. Nanotechnol.* **2006**, *1*, 60–65.
9. Bachilo, S.; Strano, M.; Kittrell, C.; Hauge, R.; Smalley, R.; Weisman, R. Structure-Assigned Optical Spectra of Single-Walled Carbon Nanotubes. *Science* **2002**, *298*, 2361–2366.
10. Hartschuh, A.; Pedrosa, H. N.; Novotny, L.; Krauss, T. D. Simultaneous Fluorescence and Raman Scattering from Single Carbon Nanotubes. *Science* **2003**, *301*, 1354–6.
11. Hagen, A.; Steiner, M.; Raschke, M.; Lienau, C.; Hertel, T.; Qian, H.; Meixner, A.; Hartschuh, A. Exponential Decay Lifetimes of Excitons in Individual Single-Walled Carbon Nanotubes. *Phys. Rev. Lett.* **2005**, *95*, 197401.
12. Korovyanko, O.; Sheng, C. X.; Vardeny, Z.; Dalton, A.; Baughman, R. Ultrafast Spectroscopy of Excitons in Single-Walled Carbon Nanotubes. *Phys. Rev. Lett.* **2004**, *92*, 17403.
13. Huang, L.; Pedrosa, H. N.; Krauss, T. D. Ultrafast Ground-State Recovery of Single-Walled Carbon Nanotubes. *Phys. Rev. Lett.* **2004**, *93*, 17403.
14. Ostojic, G.; Zaric, S.; Kono, J.; Strano, M.; Moore, V.; Hauge, R.; Smalley, R. Interband Recombination Dynamics in Resonantly Excited Single-Walled Carbon Nanotubes. *Phys. Rev. Lett.* **2004**, *92*, 117402.
15. Huang, L.; Krauss, T. D. Quantized Bimolecular Auger Recombination of Excitons in Single-Walled Carbon Nanotubes. *Phys. Rev. Lett.* **2006**, *96*, 57407.
16. Sheng, C. X.; Vardeny, Z. V.; Dalton, A. B.; Baughman, R. H. Exciton Dynamics in Single-Walled Nanotubes: Transient Photoinduced Dichroism and Polarized Emission. *Phys. Rev. B* **2005**, *71*, 125427.
17. Ma, Y.-Z.; Stenger, J.; Zimmermann, J.; Bachilo, S. M.; Smalley, R. E.; Weisman, R. B.; Fleming, G. R. Ultrafast Carrier Dynamics in Single-Walled Carbon Nanotubes Probed by Femtosecond Spectroscopy. *J. Chem. Phys.* **2004**, *120*, 3368–73.
18. Ma, Y.-Z.; Hertel, T.; Vardeny, Z. V.; Fleming, G. R.; Valkunas, L. Ultrafast Spectroscopy of Carbon Nanotubes. *Top. Appl. Phys.* **2008**, *111*, 321–352.
19. Wang, F.; Dukovic, G.; Brus, L. E.; Heinz, T. F. The Optical Resonances in Carbon Nanotubes Arise from Excitons. *Science* **2005**, *308*, 838–41.
20. Htoon, H.; Connell, M.; Doorn, S.; Klimov, V. Single Carbon Nanotubes Probed by Photoluminescence Excitation Spectroscopy: The Role of Phonon-Assisted Transitions. *Phys. Rev. Lett.* **2005**, *94*, 127403.
21. Barros, E. B.; Capaz, R. B.; Jorio, A.; Samsonidze, G. G.; Souza, A. G.; Ismail-Beigi, S.; Spataru, C. D.; Louie, S. G.; Dresselhaus, G.; Dresselhaus, M. S. Selection Rules for One- and Two-Photon Absorption by Excitons in Carbon Nanotubes. *Phys. Rev. B* **2006**, *73*, 241406.
22. Spataru, C. D.; Ismail-Beigi, S.; Capaz, R. B.; Louie, S. G. Theory and Ab Initio Calculation of Radiative Lifetime of Excitons in Semiconducting Carbon Nanotubes. *Phys. Rev. Lett.* **2005**, *95*, 247402.
23. Perebeinos, V.; Tersoff, J.; Avouris, P. Radiative Lifetime of Excitons in Carbon Nanotubes. *Nano Lett.* **2005**, *5*, 2495–2499.
24. Shaver, J.; Kono, J.; Portugall, O.; Krstic, V.; Rikken, G. L. J. A.; Miyachi, Y.; Maruyama, S.; Perebeinos, V. Magnetic Brightening of Carbon Nanotube Photoluminescence through Symmetry Breaking. *Nano Lett.* **2007**, *7*, 1851–1855.
25. Srivastava, A.; Htoon, H.; Klimov, V. I.; Kono, J. Direct Observation of Dark Excitons in Individual Carbon Nanotubes: Inhomogeneity in the Exchange Splitting. *Phys. Rev. Lett.* **2008**, *101*, 087402.
26. Ostojic, G. N.; Zaric, S.; Kono, J.; Moore, V. C.; Hauge, R. H.; Smalley, R. E. Stability of High-Density One-Dimensional Excitons in Carbon Nanotubes under High Laser Excitation. *Phys. Rev. Lett.* **2005**, *94*, 097401.
27. Ma, Y. Z.; Valkunas, L.; Dexheimer, S. L.; Bachilo, S. M.; Fleming, G. R. Femtosecond Spectroscopy of Optical Excitations in Single-Walled Carbon Nanotubes: Evidence for Exciton-Exciton Annihilation. *Phys. Rev. Lett.* **2005**, *94*, 157402.
28. Zhu, Z.; Crochet, J.; Arnold, M. S.; Hersam, M. C.; Ulbricht, H.; Resasco, D.; Hertel, T. Pump-Probe Spectroscopy of Exciton Dynamics in (6,5) Carbon Nanotubes. *J. Phys. Chem. C* **2007**, *111*, 3831–3835.
29. Lueer, L.; Hoseinkhani, S.; Polli, D.; Crochet, J.; Hertel, T.; Lanzani, G. Size and Mobility of Excitons in (6,5) Carbon Nanotubes. *Nat. Phys.* **2009**, *5*, 54–58.
30. Manzoni, C.; Gambetta, A.; Menna, E.; Meneghetti, M.; Lanzani, G.; Cerullo, G. Intersubband Exciton Relaxation Dynamics in Single-Walled Carbon Nanotubes. *Phys. Rev. Lett.* **2005**, *94*, 207401.
31. Styers-Barnett, D. J.; Ellison, S. P.; Mehl, B. P.; Westlake, B. C.; House, R. L.; Park, C.; Wise, K. E.; Papanikolas, J. M. Exciton Dynamics and Biexciton Formation in Single-Walled Carbon Nanotubes Studied with Femtosecond Transient Absorption Spectroscopy. *J. Phys. Chem. C* **2008**, *112*, 4507–4516.
32. Heller, D. A.; Mayrhofer, R. M.; Baik, S.; Grinkova, Y. V.; Usrey, M. L.; Strano, M. S. Concomitant Length and Diameter Separation of Single-Walled Carbon Nanotubes. *J. Am. Chem. Soc.* **2004**, *126*, 14567–73.
33. van Dijk, M. A.; Lippitz, M.; Orrit, M. Detection of Acoustic Oscillations of Single Gold Nanospheres by Time-Resolved Interferometry. *Phys. Rev. Lett.* **2005**, *95*, 267406.
34. Muskens, O. L.; Del Fatti, N.; Vallée, F. Femtosecond Response of a Single Metal Nanoparticle. *Nano Lett.* **2006**, *6*, 552–556.
35. Hartland, G. V. Ultrafast Studies of Single Semiconductor and Metal Nanostructures through Transient Absorption Microscopy. *Chem. Sci.* **2010**, *1*, 303–309.
36. Gao, B.; Hartland, G.; Fang, T.; Kelly, M.; Jena, D.; Xing, H. G.; Huang, L. Studies of Intrinsic Hot Phonon Dynamics in Suspended Graphene by Transient Absorption Microscopy. *Nano Lett.* **2011**, *11*, 3184–3189.
37. Jung, Y.; Slipchenko, M. N.; Liu, C. H.; Ribbe, A. E.; Zhong, Z. H.; Yang, C.; Cheng, J. X. Fast Detection of the Metallic State of Individual Single-Walled Carbon Nanotubes Using a Transient-Absorption Optical Microscope. *Phys. Rev. Lett.* **2010**, *105*, 217401.
38. Kim, H.; Sheps, T.; Collins, P. G.; Potma, E. O. Nonlinear Optical Imaging of Individual Carbon Nanotubes with

- Four-Wave-Mixing Microscopy. *Nano Lett.* **2009**, *9*, 2991–2995.
39. Myllyperkio, P.; Herranen, O.; Rintala, J.; Jiang, H.; Mudimela, P. R.; Zhu, Z.; Nasibulin, A. G.; Johansson, A.; Kauppinen, E. I.; Ahlskog, M.; Pettersson, M. Femtosecond Four-Wave-Mixing Spectroscopy of Suspended Individual Semiconducting Single-Walled Carbon Nanotubes. *ACS Nano* **2010**, *4*, 6780–6786.
40. Strano, M. S. Probing Chiral Selective Reactions Using a Revised Kataura Plot for the Interpretation of Single-Walled Carbon Nanotube Spectroscopy. *J. Am. Chem. Soc.* **2003**, *125*, 16148–16153.
41. Popov, V. N.; Henrard, L.; Lambin, P. Resonant Raman Intensity of the Radial Breathing Mode of Single-Walled Carbon Nanotubes within a Nonorthogonal Tight-Binding Model. *Nano Lett.* **2004**, *4*, 1795–1799.
42. Weisman, R. B.; Bachilo, S. M. Dependence of Optical Transition Energies on Structure for Single-Walled Carbon Nanotubes in Aqueous Suspension: An Empirical Kataura Plot. *Nano Lett.* **2003**, *3*, 1235–1238.
43. Araujo, P. T.; Doorn, S. K.; Kilina, S.; Tretiak, S.; Einarsson, E.; Maruyama, S.; Chacham, H.; Pimenta, M. A.; Jorio, A. Third and Fourth Optical Transitions in Semiconducting Carbon Nanotubes. *Phys. Rev. Lett.* **2007**, *98*, 067401.
44. Haroz, E. H.; Bachilo, S. M.; Weisman, R. B.; Doorn, S. K. Curvature Effects on the E(33) and E(44) Exciton Transitions in Semiconducting Single-Walled Carbon Nanotubes. *Phys. Rev. B* **2008**, *77*, 125405.
45. Lefebvre, J.; Austing, D. G.; Bond, J.; Finnie, P. Photoluminescence Imaging of Suspended Single-Walled Carbon Nanotubes. *Nano Lett.* **2006**, *6*, 1603–8.
46. Wang, S.; Kafizov, M.; Tu, X.; Zheng, M.; Krauss, T. D. Multiple Exciton Generation in Single-Walled Carbon Nanotubes. *Nano Lett.* **2010**, *10*, 2381–2386.
47. Pedersen, T. G.; Pedersen, K.; Cornean, H. D.; Duclos, P. Stability and Signatures of Biexcitons in Carbon Nanotubes. *Nano Lett.* **2005**, *5*, 291–294.
48. Kammerlander, D.; Prezzi, D.; Goldoni, G.; Molinari, E.; Hohenester, U. Biexciton Stability in Carbon Nanotubes. *Phys. Rev. Lett.* **2007**, *99*, 126806.
49. Chou, S.; Plentz, F.; Jiang, J.; Saito, R.; Nezich, D.; Ribeiro, H.; Jorio, A.; Pimenta, M.; Samsonidze, G.; Santos, A.; et al. Phonon-Assisted Excitonic Recombination Channels Observed in DNA-Wrapped Carbon Nanotubes Using Photoluminescence Spectroscopy. *Phys. Rev. Lett.* **2005**, *94*, 127402.
50. Zhu, Z. Ultrafast Pump Probe Spectroscopy of Single-Wall Carbon Nanotubes. In etd.library.vanderbilt.edu.
51. Tong, L.; Liu, Y.; Dolash, B. D.; Jung, Y.; Slipchenko, M. N.; Bergstrom, D. E.; Cheng, J.-X. Label-Free Imaging of Semiconducting and Metallic Carbon Nanotubes in Cells and Mice Using Transient Absorption Microscopy. *Nat. Nanotechnol.* **2011**, *7*, 56–61.
52. Yuan, D.; Ding, L.; Chu, H.; Feng, Y.; McNicholas, T. P.; Liu, J. Horizontally Aligned Single-Walled Carbon Nanotube on Quartz from a Large Variety of Metal Catalysts. *Nano Lett.* **2008**, *8*, 2576–2579.
53. Jiao, L.; Xian, X.; Wu, Z.; Zhang, J.; Liu, Z. Selective Positioning and Integration of Individual Single-Walled Carbon Nanotubes. *Nano Lett.* **2009**, *9*, 205–9.
54. Berciaud, S.; Cognet, L.; Lounis, B. Luminescence Decay and the Absorption Cross Section of Individual Single-Walled Carbon Nanotubes. *Phys. Rev. Lett.* **2008**, *101*, 77402.